Throughput Maximization For UAV-RIS NOMA Cognitive Systems in Disaster Communications

Nguyen Quoc Long, Van Nhan Vo, Viet-Hung Dang, Hung Tran, Dinh-Hieu Tran, Zhenni Pan, Shigeru Shimamoto, and Tu Dac Ho

2024 RIVF International Conference on Computing and Communication Technologies (RIVF) | 979-8-3315-0507-3/24/$31.00 ©2024 IEEE | DOI: 10.1109/RIVF64335.2024.11009076

***Abstract*—This paper examines a cognitive radio (CR) non-orthogonal multiple access (NOMA) system, which deploys an unmanned aerial vehicle (UAV) with a reconfigurable intelligent surface (RIS) in a disaster area. In particular, in the primary network, a base station (BS) communicates with a primary receiver (PR), while a secondary transmitter (ST) simultaneously sends superimposed signals to the two sensor destinations (SDs) via NOMA with the help of the UAV-RIS. Furthermore, a UAV eavesdropper (UE) wiretaps the signals from the UAV-RIS. To improve system performance, we then employ bat algorithm optimization (BAO) to maximize secondary network throughput under outage probability and security constraints.**

***Index Terms*—Cognitive Radio (CR), Nonorthogonal Multiple Access (NOMA), Unmanned Aerial Vehicle (UAV), Reconfigurable intelligent surface (RIS), Bat algorithm optimization (BAO)**

I. Introduction

Infrastructure failure is likely to disrupt traditional terrestrial cellular networks during disaster recovery and relief situations like the aftermath of flooding, hurricanes, and earthquakes [1]. Hence, there is a need for robust and dependable communication networks that facilitate data transmission in areas affected by disasters [2]. Experts have suggested various technical solutions as potential options for resolving the problem.

For example, device-to-device (D2D) networks enable packet transmission between nearby nodes without the wire network [3]. Optimizing routes between distributed nodes in disaster areas is highly challenging due to unfavorable wireless channels. Satellite communications could serve as a viable technology for emergency communications in disaster areas where terrestrial networks are unavailable [4]. However, limited and expensive resources, such as low data rates and high end-to-end latency, as well as the limited availability of equipment for the general public, hinder the widespread use of satellites.

The use of unmanned aerial vehicles (UAVs) in cellular networks has gained attention as a reliable solution for providing communication services to users on the ground in disaster areas. These UAVs offer deployment flexibility and mobility, along with adaptive altitude, to ensure reliable connectivity. When compared to older technologies, the main benefit of using UAVs as flying and adjustable-altitude relay nodes is that they can use line-of-sight (LoS) communication links to connect to multiple users [5]. In real-world applications, UAVs can play a crucial role in search and rescue missions. They can assist firefighters, police officers, and volunteer rescue teams in covering vast areas to locate missing persons, crime victims, or individuals in need of assistance, regardless of the environment. During major disasters that compromise communication infrastructure, establishing a reliable and flexible emergency communication platform for survivors poses a significant challenge in search and rescue efforts. UAVs offer an effective solution to address this critical need [6].

Furthermore, the emergence of configurable intelligent surfaces (RISs) helps the UAV improve both spectral efficiency and energy efficiency [7]. More precisely, a RIS consists of multiple passive reflecting components that collaborate to modify wireless transmission conditions from start to finish [8]. As a result, the use of RIS is efficient in conserving a UAV's energy [9]. Additionally, cognitive radio (CR) and non-orthogonal multiple access (NOMA) technologies have been found to be effective ways to make next-generation networks easier to use and less prone to interference [10]. Specifically, CR allows secondary users to opportunistically or cooperatively access the licensed spectrum band that primary users are currently using while ensuring their quality of service. This allows for more efficient use of the available wireless spectrum [11]. Recent studies [12] have demonstrated that CR offers substantial advantages, including enhanced communication quality and improved spectrum utilization.

Beside, conventional orthogonal multiple access (OMA) methods aim to reduce interference among users by assigning each user a distinct set of shared resources, such as frequency channels or time slots. Nevertheless, this constraint restricts the number of users capable of utilizing the network's resources concurrently and diminishes the network's spectrum efficiency [13]. Therefore, NOMA is a potential technique for multiple access that has the potential to enhance spectral efficiency by effectively utilizing limited spectrum resources. By combining NOMA with CR, it becomes possible to serve multiple secondary users simultaneously by adjusting their power levels and granting access to the same frequency band used by the primary network. According to [14], NOMA CR networks are expected to significantly improve spectrum utilization.

Nevertheless, NOMA CR networks faces significant security challenges due to its broadcast nature, which makes it susceptible to eavesdropping and unauthorized access. Traditional encryption techniques and access control mechanisms can mitigate these issues; however, the computational complexity of such algorithms often exceeds the capabilities of resource-constrained IoT devices. To address this limitation, physical layer security (PLS) emerges as a promising solution. By leveraging the unique characteristics of the wireless channel, such as fading and noise, PLS enhances security without imposing additional computational burdens on IoT devices, ensuring a more efficient and practical approach to safeguarding NOMA

979-8-3315-0507-3/24/$31.00 ©2024 IEEE

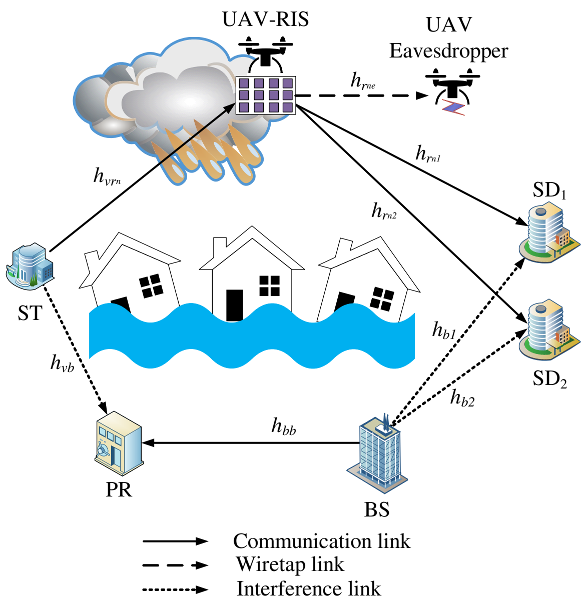

Figure 1: A UAV-RIS NOMA CR system in disaster emergency communication

CR networks [15].

However, designing NOMA CR systems requires overcoming many challenges, including low throughput and security risks. Therefore, in this paper, we maximize the throughput of UAV-RIS for the NOMA CR system in disaster emergency communications. In summary, we have made the following key contributions.

- We explore an emergency scenario where a disaster interrupts communication. Specifically, we use the UAV-RIS to establish a connection for the secondary network while simultaneously preserving communication with the primary network.
- We then define the associated optimization problem, which aims to maximize the throughput of the secondary network by determining the UAV-RIS location and many other related parameters.
- We use a population-based optimization method, i.e, bat algorithm optimization (BAO), to find the best set of system setup parameters and UAV-RIS configuration parameter for getting the best throughput while keeping system performance and security high.

We organize the remainder of this paper as follows: Section II introduces the system model and communication protocol. Section III presents the system performance metrics, the optimization problem formulation, and an optimization algorithm. The simulation results are presented and discussed in Section IV, and conclusions are given in Section V.

II. System Model and Communication Protocol

A. System model and channel assumptions

We investigate an emergency communication scenario in an area where floods and storms often occur and cause wired connections to break. In particular, we designed a NOMA CR system to establish an emergency connection from the primary base station (BS) and secondary transmitter (ST) to the primary receiver (PR) and two sensor destinations (SDs), respectively. We assume that because of the short distance, the BS can directly communicate with the PR. However, it is impossible for the ST to connect directly with the SD$_1$ and SD$_2$ due to the long distance and the obstacles; thus, the UAV-RIS with N reconfigurable reflector elements acts as a relay (called a UR) to connect the ST and its receivers [16]. In addition, a UAV eavesdropper (UE) exists to wiretap the confidential signal from the ST to its receivers due to the broadcast nature of their transmissions [15]. In order to improve the security performance, the UR sends a signal to interfere with the UE. Each device in this scenario has a single antenna. We denote the channel gain and distance of the BS–PR, ST–UR$_n$, UR$_n$–SD$_1$, UR$_n$–SD$_2$, UR$_n$–UE, BS–SD$_1$, and BS–SD$_1$ links as h_{bb} and d_{bb}, h_{vb} and d_{vb}, h_{vr_n} and d_{vr_n}, h_{r_n1} and d_{r_n1}, h_{r_n2} and d_{r_n2}, h_{b1} and d_{b1}, h_{b2} and d_{b2}, respectively, where $n \in \{1, \cdots, N\}$.

We model the channel gain for ground-to-ground communication using the gains of Rayleigh fading channels. For air-to-ground and ground-to-air communication, the path loss models are expressed as absolute values: $\overline{L}_\varsigma = \beta_\varsigma d_\varsigma^{\eta_b}$, where $\varsigma \in \{vr_n, r_n1, r_n2\}$. Specially, air-to-ground and ground-to-air communications are typically characterized by either line-of-sight (LoS) conditions or non-line-of-sight (NLoS) conditions, which depend on the specific environment, such as suburban, urban, or dense urban areas. With $\eta_\varsigma = 2$, we have $\beta_\varsigma = 10^\Gamma$, where Γ is defined as: $\Gamma = \frac{10\log_{10}(4\pi f/c)^2 + \sigma_{\text{NLoS}}}{10} + \frac{\sigma_{\text{LoS}} - \sigma_{\text{NLoS}}}{10 + 10\varphi \exp\left[-\psi\left(\frac{180}{\pi}\theta - \varphi\right)\right]}$, where θ is the elevation angle of the UR with respect to the SDs; φ and ψ are environment-dependent constants, and σ_{LoS} and σ_{NLoS} are parameters that change with frequency and environment and show the extra path losses of the LoS and NLoS links, respectively. For air-to-air communication, the path loss is given by $\overline{L}_{r_ne} = \left(\frac{4\pi f}{c}\right)^2 d_{r_ne}^{\eta_{r_ne}}$ [17].

Furthermore, the channel gains for ground-to-air, air-to-ground, and air-to-air communication follow a Nakagami-m fading model, where m represents the severity parameter of the fading environment [17]. In addition, imperfect channel state information (ICSI) is considered for all channels due to the complex environment. This means that the channel coefficients, denoted as h_α, can be expressed as the sum of their estimated values, $\tilde{h}_\alpha$ and the error terms e_α, where $\alpha \in \{\varsigma, vb, bb, b1, b2, r_ne\}$. The error terms are assumed to follow a complex normal distribution with mean zero and variance Ω_e, which represents the accuracy of the channel estimation and $e_\alpha \sim \mathcal{CN}(0, \Omega_e)$ [18].

B. Communication protocol

In the primary network, the BS uses its transmit power to send a signal $\boldsymbol{x}_B$ to the PR in orthogonal frequency bands. In the meantime, the ST transmits the confidential signal $\boldsymbol{x}_2$ to the SDs with the help of the UR in the secondary network. As a result of the CR technique, the ST interferes with the PR, resulting in the following receiver signal at the PR:

$$\boldsymbol{y}_B = \sqrt{\frac{P_B h_{bb}}{d_{bb}^\theta}} \boldsymbol{x}_B + \sqrt{\frac{P_S h_{vb}}{d_{vb}^\theta}} \boldsymbol{x}_S + \boldsymbol{n}_{\text{B}}, \quad (1)$$

where P_B and P_S are the transmit power levels of the BS and ST, respectively, and $\boldsymbol{n}_{\mathrm{V}} \sim \mathcal{CN}(0, N_0)$. Thus, the receiver signal-to-interference-plus-noise ratio (SINR) at the PR is

$$\gamma_B = \frac{\rho_B \tilde{h}_{bb}}{d_{bb}^{\theta}\left[\frac{\rho_S \tilde{h}_{vb}}{d_{vb}^{\theta}} + (\rho_B + \rho_S)\,\Omega_e + 1\right]}, \tag{2}$$

where $\rho_B = P_B/N_0$ and $\rho_S = P_S/N_0$. For the secondary network, the ST transmits the superimposed signal $\boldsymbol{x}_S$ to the SDs by using the UR, where $\boldsymbol{x}_S = \sqrt{\mu_1}\boldsymbol{x}_1 + \sqrt{\mu_2}\boldsymbol{x}_2$. Here, $\boldsymbol{x}_1$ and $\boldsymbol{x}_2$ are SD_1 and SD_2 signals, respectively; and $\mu_1 + \mu_2 = 1$ with $\mu_1 > \mu_2$.

Thus, the signal received at the SD_1 and SD_2 under interference from the BS can be described as

$$\boldsymbol{y}_{\mathrm{SD}_1} = \sum_{n=1}^{N} \sqrt{\frac{P_S h_{vr_n} h_{r_n 1}}{\bar{L}_{vr_n}\bar{L}_{r_n 1}}}\boldsymbol{x}_S + \sqrt{\frac{P_B h_{b1}}{d_{b1}^{\theta}}}\boldsymbol{x}_B + n_1, \tag{3}$$

$$\boldsymbol{y}_{\mathrm{SD}_2} = \sum_{n=1}^{N} \sqrt{\frac{P_S h_{vr_n} h_{r_n 2}}{\bar{L}_{vr_n}\bar{L}_{r_n 2}}}\boldsymbol{x}_S + \sqrt{\frac{P_B h_{b2}}{d_{b2}^{\theta}}}\boldsymbol{x}_B + n_2, \tag{4}$$

where $\boldsymbol{n}_1, \boldsymbol{n}_2 \sim \mathcal{CN}(0, N_0)$. Under the NOMA scheme, SD_1 directly decodes its signal by treating the signal for SD_2 as noise, yielding the following SINR as

$$\gamma_{\mathrm{SD}_1} = \frac{\Delta_{11}}{\Delta_{11} + \frac{\rho_B \tilde{h}_{b1}}{d_{b1}^{\theta}} + (\rho_B + \Delta_{13})\,\Omega_e + 1}, \tag{5}$$

where Δ_{11}, Δ_{12}, and Δ_{13} are defined as

$$\Delta_{11} = \sum_{n=1}^{N} \frac{\mu_1 \rho_S \tilde{h}_{vr_n}\tilde{h}_{r_n 1}}{\bar{L}_{vr_n}\bar{L}_{r_n 1}}, \tag{6}$$

$$\Delta_{12} = \sum_{n=1}^{N} \frac{\mu_2 \rho_S \left(\tilde{h}_{vr_n} + \Omega_e\right)\left(\tilde{h}_{r_n 1} + \Omega_e\right)}{\bar{L}_{vr_n}\bar{L}_{r_n 1}}, \tag{7}$$

$$\Delta_{13} = \sum_{n=1}^{N} \frac{\mu_1 \rho_S \left(\tilde{h}_{vr_n} + \tilde{h}_{r_n 1} + \Omega_e\right)}{\bar{L}_{vr_n}\bar{L}_{r_n 1}}. \tag{8}$$

Meanwhile, SD_2 should first decode the signal $\boldsymbol{x}_1$ by treating $\boldsymbol{x}_2$ as noise and then remove $\boldsymbol{x}_1$ to obtain $\boldsymbol{x}_2$ from the superimposed signal using successive interference cancellation (SIC) [16]. Here, we consider imperfect SIC at SD_2 due to residual interference caused by potential deployment problems (such as error propagation and complexity scaling). These unwanted decoding errors are the primary reason for the performance degradation. Thus, the NOMA network will be affected by residual interference through signal errors because of imperfect SIC. Specifically, the interference term due to imperfect SIC is $I_S \sim \mathcal{CN}(0, \xi_S N_0)$ [14]. When $\boldsymbol{x}_1$ is successfully decoded, the received SINR at SD_2 is represented as follows:

$$\gamma_{\mathrm{SD}_2} = \frac{\Delta_{21}}{\frac{\rho_P \tilde{h}_{b2}}{d_{b2}^{\theta}} + [\rho_B + \Delta_{22}]\,\Omega_e + I_S + 1}, \tag{9}$$

where Δ_{21} and Δ_{22} are defined as

$$\Delta_{21} = \sum_{n=1}^{N} \frac{\mu_2 \rho_S \tilde{h}_{sr_n}\tilde{h}_{r_n 2}}{\bar{L}_{sr_n}\bar{L}_{r_n 2}}, \tag{10}$$

$$\Delta_{22} = \sum_{n=1}^{N} \frac{\mu_2 \rho_B \left(\tilde{h}_{sr_n} + \tilde{h}_{r_n 2} + \Omega_e\right)}{\bar{L}_{sr_n}\bar{L}_{r_n 2}}. \tag{11}$$

Similarly, the SINRs at the UE to wiretap x_1 and x_2 are as follows:

$$\gamma_{\mathrm{E}_1} = \frac{\Delta_{e1}}{\Delta_{e12} + \Delta_{e13}\Omega_e + 1}, \tag{12}$$

$$\gamma_{\mathrm{E}_2} = \frac{\Delta_{e21}}{\Delta_{e22}\Omega_e + I_S + 1}, \tag{13}$$

where Δ_{e11}, Δ_{e12}, Δ_{e13}, Δ_{e21}, and Δ_{e22} are

$$\Delta_{e11} = \sum_{n=1}^{N} \frac{\mu_1 \rho_S \tilde{h}_{vr_n}\tilde{h}_{r_n e}}{\bar{L}_{vr_n}\bar{L}_{r_n e}}, \tag{14}$$

$$\Delta_{e12} = \sum_{n=1}^{N} \frac{\mu_2 \rho_S \left(\tilde{h}_{vr_n} + \Omega_e\right)\left(\tilde{h}_{r_n e} + \Omega_e\right)}{\bar{L}_{vr_n}\bar{L}_{r_n e}}, \tag{15}$$

$$\Delta_{e13} = \sum_{n=1}^{N} \frac{\mu_1 \rho_S \left(\tilde{h}_{vr_n} + \tilde{h}_{r_n e} + \Omega_e\right)}{\bar{L}_{vr_n}\bar{L}_{r_n e}}, \tag{16}$$

$$\Delta_{e21} = \sum_{n=1}^{N} \frac{\mu_2 \rho_S \tilde{h}_{sr_n}\tilde{h}_{r_n e}}{\bar{L}_{sr_n}\bar{L}_{r_n e}}, \tag{17}$$

$$\Delta_{e22} = \sum_{n=1}^{N} \frac{\mu_2 \rho_S \left(\tilde{h}_{sr_n} + \tilde{h}_{r_n e} + \Omega_e\right)}{\bar{L}_{sr_n}\bar{L}_{r_n e}}. \tag{18}$$

III. Performance Metrics, Problem Formulation, and Throughput Optimization

In this section, we formulate the throughput of the secondary network, the outage probability of the primary network, and the leakage probability at the UE. Next, we present our optimization problem statement, in which BS and ST must regulate their power consumption and position in the UR to ensure primary network communication. Furthermore, this statement maximizes the secondary network's throughput and guarantees its secrecy performance.

First, the outage probability of the secondary network is defined as the channel capacity of either SD_1 or SD_2 falling below the outage target rate R_S. This means that

$$\mathcal{O}_S = \Pr\left\{C_{\mathrm{SD}_1} < R_S \text{ or } C_{\mathrm{SD}_2} < R_S\right\}, \tag{19}$$

where $\Pr\{\cdot\}$ is the probability function and C_{SD_1} and C_{SD_2} are the channel capacities of the ST→SD_1 and ST→SD_2 links with system bandwidth (W), expressed as $C_{\mathrm{SD}_1} = W\log_2\left(1 + \gamma_{\mathrm{SD}_1}\right)$ and $C_{\mathrm{SD}_2} = W\log_2\left(1 + \gamma_{\mathrm{SD}_2}\right)$, respectively. Therefore, we formulate the secondary network's throughput as $\mathcal{T} = R_S \times (1 - \mathcal{O}_S)$. Similar to (19), the outage probability of the primary network is given by:

$$\mathcal{O}_B = \Pr\left\{C_B < R_B\right\}, \tag{20}$$

where R_B is the outage target rate at the PR and C_B is the channel capacity of the BS→PR link, expressed as $C_B = W\log_2\left(1 + \gamma_B\right)$. Furthermore, the PLS is investigated to evaluate the secrecy performance. In particular, the leakage probability at the UE is defined as the channel capacity from the UR to the UE for decoding either x_1 or x_2 higher than the leakage rate R_E, i.e.,

$$\mathcal{L} = \Pr\left\{C_{E_1} > R_E \text{ or } C_{E_2} > R_E\right\}, \quad (21)$$

where C_{E_1} and C_{E_2} are the channel capacities of the UR→UE link to decode x_1 and x_2, expressed as $C_{E_1} = W\log_2(1+\gamma_{E_1})$ and $C_{E_2} = W\log_2(1+\gamma_{E_2})$, respectively. Finally, our main goal is to maximize the secondary network's throughput while ensuring that two constraints are met: the PR can receive and decode their required signals, but the UE cannot fully decode the superimposed signal. In particular, the first constraint ensures that the outage probability of the PR is lower than a predefined threshold ϵ_B, i.e., $\mathcal{O}_B < \epsilon_B$. Similarly, the second constraint guarantees that the leakage probability at the UE is less than ϵ_E, i.e., $\mathcal{L} < \epsilon_E$.

Based on this, we formulate an optimization problem that aims to determine not only the UR location but also many other related parameters. In particular, we optimize the transmit power levels of the BS, ST, and the 3-D position of the UR. Therefore, we can formulate the optimization problem as follows:

$$\max_{\boldsymbol{d}} \{\mathcal{T}\}, \quad (22)$$

$$\text{s.t. } \mathcal{O}_B < \epsilon_B, \quad (23)$$

$$\mathcal{L} < \epsilon_E, \quad (24)$$

where $\boldsymbol{d}$ is the vector of parameters to be optimized, including N, P_B, P_S, and the coordinates of the UR (x_n, y_n, h_n), that is defined as $\mathbf{d} = [N, P_B, P_S, x_n, y_n, z_n]$.

Note that the optimization problem defined in (22) is nonconvex in terms of both the objective value and the constrained domain, and the search space has 6 dimensions. More specifically, BAO is used to solve the problem defined in (22) [19]. The optimized parameters are organized into a candidate vector, or a virtual bat, as $\mathbf{d}$. The BAO algorithm first generates the initial population of N candidates with the form of $\mathbf{d}$. Each candidate $\mathbf{d}_i$ will have its respective velocity v_i, pulse rate r_i, pulse frequency f_i, and loudness a_i. Then, in each generation:

- All the bats' fitness values are evaluated.
- The bat $\mathbf{d}_i$ increases frequency higher if it finds a good prey or achieves high value of fitness. It also updates its velocity based on its old velocity (as the momentum) and the pulling force towards the best bat's position. Then, due to its new velocity, the bat $\mathbf{d}_i$ updates its position.
- Each bat generates its potential, replacing version $\mathbf{d'}_i$ with the probability of $(1-r_i)$. This is called potential because it is not always allowed to replace $\mathbf{d}_i$, but at a probability of a_i. If $\mathbf{d'}_i$ is accepted, then the bat $\mathbf{d'}_i$ replaces $\mathbf{d}_i$, resulting in an increased pulse rate and a decreased loudness.
- After a certain number of generations, the loop stops, or the average fitness value does not change for several generations.

With the modification of taking constraints into account, the objective value can be rewritten as a function of the fitness value:

$$F(\mathbf{d}) = \Upsilon_{SR_u}(\mathbf{d}) - \theta_1 \max[0, \mathcal{O}_{P_{i^*}}(\mathbf{d}) - \epsilon_P] - \theta_2 \max[0, \mathcal{O}_{SR_S}(\mathbf{d}) - \epsilon_S], \quad (25)$$

where $\theta_i > 0$, $i = 1, 2$, implying that if the constraints are not met, the fitness value is reduced proportional to θ_i.

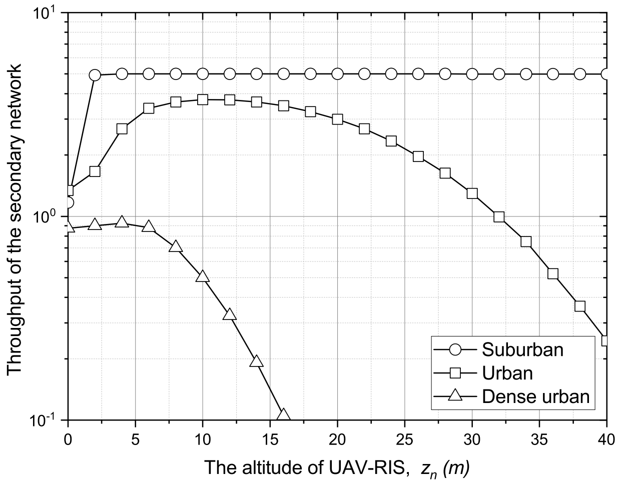

Figure 2: Throughput of the secondary network versus z_n for different environments.

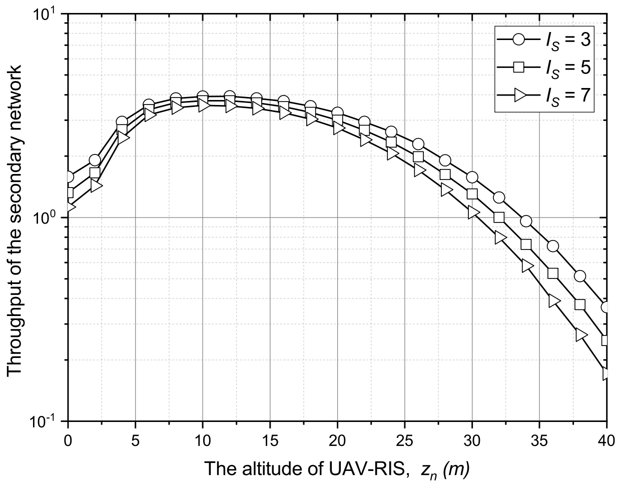

Figure 3: Throughput of the secondary network versus z_n for different I_S values.

IV. Simulation Results and Analysis

In this section, we analyze the secrecy performance in terms of leakage probability and the system performance in terms of the outage probability and throughput in the primary and secondary networks, respectively. Finally, we present BAO in optimizing the secondary network's throughput, subject to the constraints shown in (22).

According to [20], we evaluate the UAV-RIS CR-NOMA system with the following system parameters: We set the fading parameters to $m = 2$, the system bandwidth to $W = 1$ MHz, the number of reflecting elements at the UR to $N \in \{3, 5, 7\}$, and the thresholds of the PR and SD for successfully decoding their signals are given

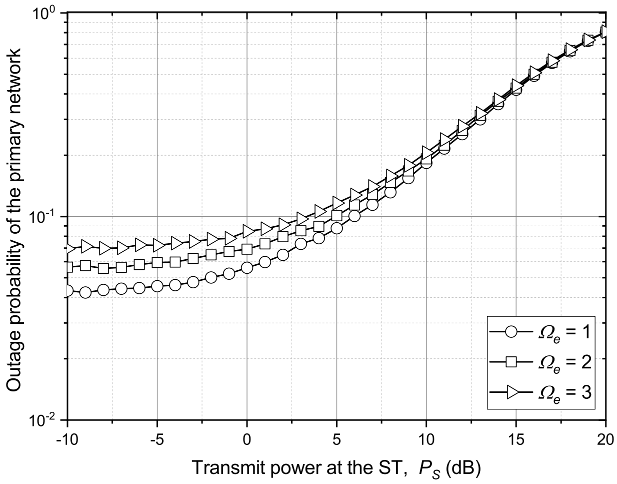

Figure 4: Outage probability of the primary network versus P_S for different Ω_e values.

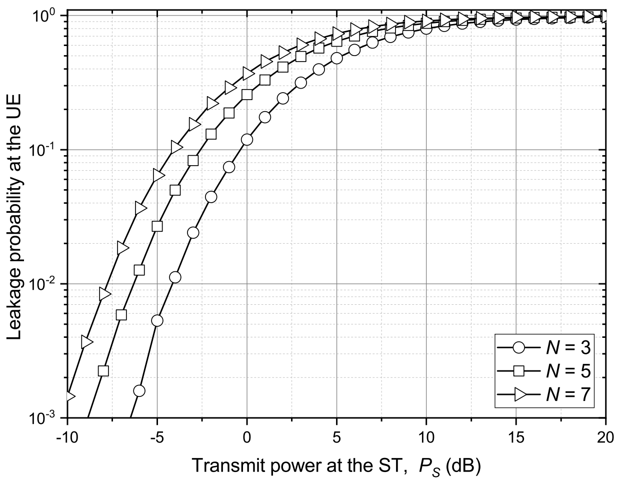

Figure 5: leakage probability at the UE versus P_S for different N values.

by $R_B = 40$ and $R_V = 5$, respectively. We set the UE leakage threshold to $R_E = 20$ and the transmit power levels of the BS, ST $P_B, P_S \in [-10, 20]$ (dB). Furthermore, we examine the performance of the UAV-RIS CR-NOMA system in various environments, including suburban, urban, and dense urban areas, using the parameters: $\varphi = [4.8860, 9.6177, 12.0870]$, $\psi = [0.4290, 0.1581, 0.1139]$, $\theta_{\text{LoS}} = [0.1, 1, 1.6]$, and $\theta_{\text{NLoS}} = [21, 20, 23]$, as provided in [21].

Firstly, we evaluate the results of secrecy and system performance in Figures 2, 3, 4, and 5. In particular, Figure 2 illustrates the impact of UAV altitude and environmental conditions (suburban, urban, and dense urban) on the throughput of the secondary network. It is observed that the throughput in suburban environments is higher than in urban and dense urban environments. This is because the probability of a LoS connection is higher in suburban areas compared to urban and dense urban areas.

Then, we investigate the considered metrics with the urban environment in the rest of the numerical results.

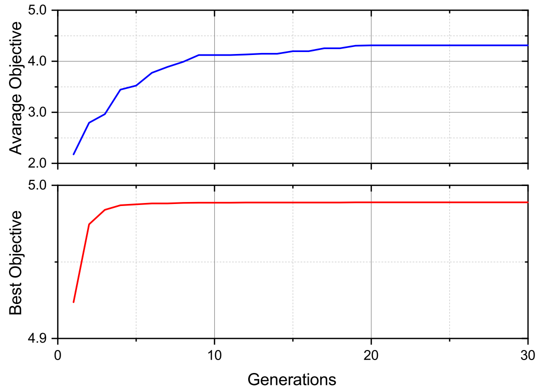

Figure 6: BAO convergence over generations

Figure 3 shows how the UR altitude and imperfect SIC parameter I_S affect the secondary network's throughput. We can see that the throughput reaches an optimal point if z_n is around 10 m. This is because if the UR flies close to the ground, the NLoS will be large, and if the UR flies too high, the path loss will be huge. Figure 4 illustrates the effects of the transmit power of the ST and the correctness of the channel estimation on the outage probability of the primary network. It is observed that the outage probability of the primary network increases once the P_B increases. This is due to the ST interfering with the PR, which is caused by the CR technique. Furthermore, in Figures 3 and 4, the system performance will improve with low I_S and Ω_e. This is a fact that the SIC and CSI are in perfect condition if I_S and Ω_e asymptote 0. Figure 5 plots the leakage probability at the UE with different transmit power levels at the ST, as well as the number of reconfigurable reflector elements N. It is shown that large N and P_S enable the UE to wiretap the confidential data more easily. Furthermore, based on Figures 4 and 5, we can see that the outage probability of the primary network and the leakage probability at the UE are high once P_S and N increase. This necessitates the adjustment of system parameters to maintain optimal system and secrecy performance.

Next, we set the constraints $\epsilon_B = 0.1$ and $\epsilon_E = 0.1$ to ensure system and secrecy performance. We then evaluate the results of the optimization method in Figure 6, with the bat number of 40 for 30 generations. It can be seen that both the average objective value of the population and the objective value of the best bat in the population increase and converge over generations. This means BAO works properly for our optimization problem. We average the results after 20 runs to highlight the trends and smooth the curve. The best-found solution provides a throughput of 4.9889 without any constraint violations. Obviously, it is recommended to use BAO in models and scenarios similar to those in this paper.

V. Conclusions

In this paper, we examined a NOMA CR system, bolstered by a UAV-RIS in the presence of the UE. To investigate system performance, we took into account the primary network's outage probability and the secondary network's throughput. In addition, we formulated the leakage probability at the UE. Finally, under the outage probability and security constraints, we applied the BAO algorithms to determine the optimal system and UAV-RIS configuration parameters. In future work, we will focus on analyzing energy consumption in UAV-RIS systems, addressing battery limitations through energy-efficient routing and resource allocation strategies to extend operational times, and developing models that account for dynamic UAV movement while tackling challenges like obstacle navigation and maintaining UAV stability.

ACKNOWLEDGMENTS

This work was supported by JST ASPIRE Grant Number JPMJAP2326, Japan and Duy Tan University.

REFERENCES

[1] D. G. C., A. Ladas, Y. A. Sambo, H. Pervaiz, C. Politis, and M. A. Imran, "An overview of post-disaster emergency communication systems in the future networks," *IEEE Wireless Commun.*, vol. 26, no. 6, pp. 132–139, 2019.

[2] T. Do-Duy, L. D. Nguyen, T. Q. Duong, S. R. Khosravirad, and H. Claussen, "Joint optimisation of real-time deployment and resource allocation for uav-aided disaster emergency communications," *IEEE J. Selected Areas in Commun.*, vol. 39, no. 11, pp. 3411–3424, 2021.

[3] A. Masaracchia, L. D. Nguyen, T. Q. Duong, and M.-N. Nguyen, "An energy-efficient clustering and routing framework for disaster relief network," *IEEE Access*, vol. 7, pp. 56 520–56 532, 2019.

[4] F. A. Tondo, M. Afhamisis, S. Montejo-Sánchez, O. L. A. López, M. R. Palattella, and R. D. Souza, "Multiple channel lora-to-leo scheduling for direct-to-satellite iot," *IEEE Access*, vol. 12, pp. 30 627–30 637, 2024.

[5] J. Guo, G. Liu, Q. Wu, and P. Fan, "Parallel attention-based transformer for channel estimation in RIS-aided 6G wireless communications," *IEEE Trans. Veh. Tech.*, pp. 1–14, 2024.

[6] M. Ghamari, P. Rangel, M. Mehrubeoglu, G. S. Tewolde, and R. S. Sherratt, "Unmanned aerial vehicle communications for civil applications: A review," *IEEE Access*, vol. 10, pp. 102 492–102 531, 2022.

[7] E. B. et al., "Reconfigurable intelligent surfaces for 6G: Emerging hardware architectures, applications, and open challenges," *IEEE Veh. Tech. Magazine*, pp. 2–22, 2024.

[8] A.-T. Le, T. D. Hieu, T. N. Nguyen, T.-L. Le, S. Q. Nguyen, and M. Voznak, "Physical layer security analysis for RIS-aided NOMA systems with non-colluding eavesdroppers," *Computer Communications*, vol. 219, pp. 194–203, 2024.

[9] H. Ren, Z. Zhang, Z. Peng, L. Li, and C. Pan, "Energy minimization in RIS-assisted UAV-enabled wireless power transfer systems," *IEEE Internet of Things J.*, vol. 10, no. 7, pp. 5794–5809, Apr. 2023.

[10] A. U. Khan, G. Abbas, Z. H. Abbas, M. Bilal, S. C. Shah, and H. Song, "Reliability analysis of cognitive radio networks with reserved spectrum for 6G-IoT," *IEEE Trans. Network and Service Management*, vol. 19, no. 3, pp. 2726–2737, 2022.

[11] Z. Xiang, W. Yang, Y. Cai, Z. Ding, and Y. Song, "Secure transmission design in HARQ assisted cognitive NOMA networks," *IEEE Trans. Inf. Forensics Secur.*, vol. 15, pp. 2528–2541, Jan. 2020.

[12] O. Hashash, W. Saad, M. F. Imani, and D. R. Smith, "Simultaneous transmitting and reflecting (STAR)-RIS for harmonious millimeter wave spectrum sharing," in *IEEE Wireless Communications and Networking Conference (WCNC)*, Glasgow, United Kingdom, Mar. 2023, pp. 1–6.

[13] Z. Chen, Z. Ding, X. Dai, and R. Zhang, "A mathematical proof of the superiority of NOMA compared to conventional OMA," *IEEE Trans. Signal Process.*, pp. 1–28, Oct. 2016.

[14] D.-T. Do, A.-T. Le, and B. M. Lee, "NOMA in cooperative underlay cognitive radio networks under imperfect SIC," *IEEE Access*, vol. 8, pp. 86 180–86 195, May 2020.

[15] V. N. Vo, H. Tran, and C. So-In, "Enhanced intrusion detection system for an EH IoT architecture using a cooperative UAV relay and friendly UAV jammer," *IEEE/CAA J. of Automatica Sinica*, vol. 8, no. 11, pp. 1786–1799, 2021.

[16] A. Bhowmick, S. Roy, and S. Kundu, "Throughput maximization of a UAV assisted CR network with NOMA-based communication and energy-harvesting," *IEEE Trans. Vehicular Tech.*, vol. 71, no. 1, pp. 362–374, Jan. 2022.

[17] B. Ji, Y. Li, S. Chen, C. Han, C. Li, and H. Wen, "Secrecy outage analysis of UAV assisted relay and antenna selection for cognitive network under nakagami-m channel," *IEEE Trans. Cognitive Commun. and Networking*, vol. 7, pp. 1–11, Jan. 2020.

[18] V. N. Vo, C. So-In, H. Tran, D. D. Tran, and T. P. Huu, "Performance analysis of an energy-harvesting IoT system using a UAV friendly jammer and NOMA under cooperative attack," *IEEE Access*, vol. 8, pp. 221 986–222 000, 2020.

[19] Y. Luo, C. Wu, Y. Leng, N. Huang, L. Mao, and J. Tang, "Throughput Optimization for NOMA Cognitive Relay Network with RF Energy Harvesting Based on Improved Bat Algorithm," *Mathematics*, vol. 10, no. 22, 2022.

[20] P. Yang, L. Yang, and S. Wang, "Performance analysis for RIS-aided wireless systems with imperfect CSI," *IEEE Wireless Commun. Letters*, vol. 11, no. 3, pp. 588–592, Mar. 2022.

[21] A. M. Hayaneh, S. A. R. Zaidi, D. C. Mclernon, M. D. Renzo, and M. Ghogho, "Performance analysis of UAV enabled disaster recovery networks: A stochastic geometric framework based on cluster processes," *IEEE Access*, vol. 6, pp. 26 215–26 230, Jun. 2018.